Comparisons of Ocean Radiative Transfer Models With SMAP and AMSR2 Observations

Lise Kilic, Catherine Prigent, Jacqueline Boutin, Thomas Meissner, Stephen English, Simon H. Yueh

Comparisons of Ocean Radiative Transfer Models with SMAP and AMSR2 Observations

Lise Kilic[1], Catherine Prigent[1,2], Jacqueline Boutin[3], Thomas Meissner[4], Stephen English[5], Simon Yueh[6]

[1]Sorbonne Université, Observatoire de Paris, Université PSL, CNRS, LERMA, Paris, France
[2]Estellus, Paris, France
[3]Sorbonne Université, CNRS, IRD, MNHN, LOCEAN, Paris, France
[4]Remote Sensing Systems, Santa Rosa, California, USA
[5]European Centre for MediumRange Weather Forecasts, Reading, UK
[6]NASA Jet Propulsion Laboratory, California Institute of Technology, Pasadena, California, USA

Key Points:

- Ocean radiative transfer simulations are compared with satellite observations from 1.4 to 89 GHz
- The analysis focuses on the accuracy of the models as a function of key ocean variables
- Major discrepancies are found for strong wind speeds and cold sea surface temperatures

Corresponding author: Lise Kilic, `lise.kilic@obspm.fr`

Abstract

The sea surface temperature (SST), ocean wind speed (OWS) and sea surface salinity (SSS) are fundamental variables for understanding, monitoring and predicting the state of the ocean and atmosphere. The analysis of these ocean parameters from passive microwave satellite measurements requires a Radiative Transfer Model (RTM). In this study, we compare three ocean RTMs from 1.4 to 89 GHz. A dataset of satellite observations from SMAP and AMSR2 collocated with surface and atmospheric parameters from ECMWF ERA-Interim and Mercator reanalysis has been developed. The selected ocean RTMs are: LOCEAN a physical model with parameters adjusted to L-band measurements, FASTEM (FAST microwave Emissivity Model) a fast parameterized model, and RSS (Remote Sensing Systems) an empirical model fitting satellite observations. Global systematic errors between simulations and observations tend to increase with frequency, and are generally higher at horizontal than at vertical polarizations. Then, the analysis focuses on the accuracy of the RTMs as a function of the key ocean variables, SST, SSS, and OWS. Major discrepancies are found at frequencies above 1.4 GHz, for OWS higher than 7 m/s, with the LOCEAN and the FASTEM models, with differences strongly increasing with increasing OWS. Cold SSTs are identified as a source of disagreement between the simulations and the observations, regardless of the model. This is a critical issue, especially at 6 GHz which is the key channel for the SST analysis from satellite. The present study is the first step toward the development of a new physically-based community model.

Plain Language Summary

The sea surface temperature, ocean wind speed, and sea surface salinity are fundamental variables for understanding, monitoring and predicting the state of the ocean and atmosphere. The analysis of these ocean parameters from passive microwave satellite measurements requires a radiative transfer model. In this study, we compare three different ocean radiative transfer models from 1.4 to 89 GHz. The analysis focuses on the accuracy of the radiative transfer models as a function of the key ocean variables. Major discrepancies with the observations are found at frequencies above 1.4 GHz, for wind speeds higher than 7 m/s, for two of the three models. Cold sea surface temperatures are also identified as a source of disagreement between the simulations and the observations, regardless of the model. The present study is the first step toward the development of a new physically-based community sea surface emissivity model.

1 Introduction

Observation of the ocean is important for oceanic forecasting, Numerical Weather Prediction (NWP), oceanic circulation, mesoscale analysis, and for the study and modeling of climate change. The Sea Surface Temperature (SST), the Sea Surface Salinity (SSS), and the Ocean Wind Speed (OWS) are fundamental variables for the ocean characterization. These variables can be analyzed from satellite observations with spatial resolution, time sampling, and uncertainty that differ upon the sensor type.

SST is a key input to atmospheric and oceanic forecasting in NWP systems (e.g., Bell et al. (2000); Martin et al. (2007)) and helps to better characterize the air-sea interaction. "All-weather" SST is required for NWP and other meteorological applications. The most important characteristics of SST analyses are not only their uncertainty, but also their ability to represent fine scale horizontal structures and their time evolution (Chelton & Wentz, 2005). Infrared sensors such as the Advanced Very-High-Resolution Radiometer (AVHRR) can retrieve SST at fine scale resolution (1 km), but only for clear sky conditions. Cloud contamination is particularly problematic as it covers ∼70% of the globe in average at all the time. Microwaves can provide "all-weather" SST with their low sen-

sitivity to clouds and aerosols, at frequencies < 12 GHz. The current Advanced Microwave Scanning Radiometer 2 (AMSR2) (Imaoka et al., 2010), which observes at frequencies between 6.9 and 89 GHz, provides SST with a spatial resolution of 50 km and a precision of 0.55 K (Gentemann & Hilburn, 2015).

SSS measurements are important for the study of the ocean dynamics, the marine biogeochemistry (Carmack et al., 2016), and the global hydrological cycle (Reul et al., 2014). Variations of the SSS force the global thermohaline circulation. Small variations in SSS may modify the vertical stratification in ocean density and thus strongly influence the ocean-atmosphere exchanges. Moreover, SSS is a passive tracer of freshwater flows from river discharges, melting ice, and ocean-atmosphere exchanges. SSS was first retrieved from space from the Soil Moisture and Ocean Salinity (SMOS) mission (launched in November 2009), using passive microwave observations at 1.4 GHz (Kerr et al., 2010). It has been followed by the Aquarius mission launched in June 2011 (Lagerloef et al., 2008), and the Soil Moisture Active Passive (SMAP) mission launched in January 2015 (Fore et al., 2016).

OWS determines the air-sea interactions, such as surface stress, sensible heating, evaporation, and gas exchange (Atlas et al., 2011). Generally, OWS and wind direction are retrieved from microwave scatterometers with 12-25 km spatial resolution, and Synthetic Aperture Radar with 500 m spatial resolution with an uncertainty of less than 2 m/s (Monaldo et al., 2014). It is also possible to derive OWS from passive microwave observations but with less sensitivity to the wind direction.

The analysis of these ocean parameters from passive microwave satellite measurements requires a Radiative Transfer Model (RTM) in order to interpret the satellite Brightness Temperatures (TBs) in terms of SST, SSS, and OWS. Ocean RTMs are developed to be applicable over a large range of frequencies, incidence angles and conditions but sometimes they are fine-tuned for a specific application and/or instrument, i.e., a selected range of frequencies and incidence angles. For the first time, with the Copernicus Imaging Microwave Radiometer (CIMR) mission (Kilic et al., 2018), 1.4 GHz (L-band) observations will be combined with 6.9, 10.6, 18.7 and 36.5 GHz (C, X, Ku, and Ka-bands) observations and will provide coincident SST, SSS, and OWS measurements. Therefore, an evaluation of the existing RTMs working at these frequencies is needed, with comparisons against satellite observations. Section 2 describes the selected ocean RTMs and the collocated surface and atmospheric datasets used to compare the RTM simulations with SMAP and AMSR2 observations. Section 3 presents the differences between observed and simulated TBs for frequencies from 1.4 to 89 GHz as a function of SST, SSS, and OWS. In section 4, we discuss possible approches to improve the ocean RTMs. Section 5 concludes this study.

2 Materials and Methods

2.1 Ocean Radiative Transfer Models

The microwave ocean emissivity varies with the Sea Surface Temperature (SST), the Ocean Wind Speed (OWS), and the Sea Surface Salinity (SSS), with sensitivities that depend upon the frequency, the polarization, and the incidence angle of observation (Wilheit & Chang, 1980). There are essentially three classes of emissivity models. Firstly, there are physical models, although some of their components may be empirically tuned: they tend to rigorously represent the complex physical interactions between the ocean surface and the radiation and are generally rather slow. Secondly, there are fast models that attempt to replicate the results of the previous physical models, using parameterizations. Lastly, there are empirical models, partly derived from matchups between in situ ocean observations and satellite observations.

Usually, an ocean RTM has three main components 1) a dielectric model, 2) a roughness model, 3) an ocean foam model. The dielectric constant needed to simulate the emissivity of a flat surface depends on the SST, the SSS, and the frequency. Dielectric constant models are expressed as a Debye law (Debye, 1929) with coefficients that have been adjusted to observations. Some dielectric constant models use a double Debye formula to extend the range of frequencies where the model is valid. A roughness model is then needed to simulate the effect of the wind-induced roughness on the ocean. Here, different types of model can be applied. The geometric optic models consider the large scale waves as an ensemble of facets with different slopes for which the Fresnel reflection applies. The double scale models consider the diffusion by the small-scale roughness on each large-scale wave, in addition to the large scale model. Then, when the steepness ratio of the waves is too large, the waves break and foam appears. The presence of foam is characterized by (1) a foam cover that depends on the OWS and is usually written as a power law (Monahan & O'Muircheartaigh, 1980), and (2) a foam emissivity that depends on frequency and incidence angle.

In this study, three ocean RTMs are compared. They are representative of the three model classes:

- The Laboratoire d'Océanographie et du Climat (LOCEAN) RTM is a full physical model adjusted to L-band observations. It was implemented by Emmanuel Dinnat and Xiaobin Yin at LOCEAN (Dinnat et al., 2003; Yin et al., 2016). It is derived from the two-scale model of Yueh (1997). The dielectric constant stems from Klein and Swift (1977), the roughness model uses the wave spectrum from Durden and Vesecky (1985) with an amplitude coefficient multiplied by 1.25 (Yin et al., 2012). The foam cover model follows Yin et al. (2016), and the foam emissivity model is from M. D. Anguelova and Gaiser (2013). This model was primarily designed for the analysis of SMOS L-band observations. Its physical basis is nevertheless generic and makes it applicable to a large range of frequencies.
- The FAST microwave Emissivity Model (FASTEM) is a fast linear regression fit to the output of a physical two scale model (English & Hewison, 1998; Liu et al., 2011). It is distributed with the RTTOV, the community radiative transfer code (Saunders et al., 1999, 2018). It was primarily developed for the assimilation of surface-sensitive microwave satellite observations in NWP centers, at frequencies above 6 GHz. FASTEM version 5 is used here. The fast linear regression fits the output of a physical two scale model in which the dielectric constant model is described in Liu et al. (2011), derived from the permittivity model of Ellison et al. (1998) and adapted with a double Debye relaxation. The roughness model is based on the wave spectrum of Durden and Vesecky (1985) with an amplitude coefficient multiplied by 2. The foam cover model is from Monahan and O'Muircheartaigh (1986). The foam emissivity is described in Liu et al. (2011): it is a combination of the adjustments of Kazumori et al. (2008) and Stogryn (1972).
- The Remote Sensing Systems (RSS) model is essentially fitted to satellite observations. It is developed with SSM/I and WindSat observations between 6-89 GHz (Meissner & Wentz, 2004, 2012) and with Aquarius observations at 1.4 GHz (Meissner et al., 2014, 2018). For the flat sea surface emissivity, it adopts the dielectric constant model of Meissner and Wentz (2004), adjusted in Meissner and Wentz (2012). The wind-induced emissivity is fitted to satellite observations and described by a polynomial function: it includes the roughness model as well as the foam contribution. For the RSS model, there are two wind-induced emissivity parameterizations : one between 6 and 90 GHz based on WindSat and SSMI F13 observations (Meissner & Wentz, 2012), and one at 1.4 GHz based on Aquarius observations (Meissner et al., 2014, 2018).

The sensitivity of the TBs to the key oceanic parameters is calculated for the selected channels. For the three RTMs, Figure 1 shows the derivative of the TB as a func-

Table 1. Summary of the selected ocean Radiative Transfer Models (RTMs).

RTM	Model type	Dielectric constant	Wave spectrum	Foam cover	Foam emissivity
LOCEAN Dinnat et al., 2003	Full physical model adjusted for L-band	Klein and Swift, 1977	Durden and Vesecky, 1985 with $a_0 \times 1.25$	Yin et al. 2016	Anguelova and Gaiser, 2013
FASTEM Liu et al., 2011	Parameterized and fast	Ellison et al., 1998 +Double Debye	Durden and Vesecky, 1985 with $a_0 \times 2$	Monahan and O'Muircheartaigh 1986	Kazumori et al., 2008 with Stogryn,1972
RSS Meissner and Wentz, 2012	Empirically fitted to observations	Meissner and Wentz, 2004 and 2012	Wind induced emissivity fitted to observations Meissner and Wentz, 2012 Meissner et al., 2014		

tion of SST, SSS, and OWS (also called the Jacobians), for the selected window frequencies, an incidence angle of 55^o, and the two orthogonal polarizations. The considered oceanic situation is close to the global mean state. The most sensitive frequency to the SST is the 6 GHz (especially in the vertical polarization), followed by the 10 GHz and the 18 GHz. The sensitivity to OWS increases with frequency in the horizontal polarization (limited sensitivity at the vertical polarization). The 1.4 GHz frequency is the most sensitive to the SSS. As a consequence and as expected, the analysis of the SST from satellite observations will rely on the 6 GHz observations, coupled with observations at 10 and/or 18 GHz: the accuracy of the RTM at these frequencies will be particularly critical for the estimation of this ocean parameter. The sensitivity of these frequencies to the OWS will also have to be accounted for in the analysis. For the analysis of the SSS, the constraints on the 1.4 GHz RTM uncertainties are very stringent, as this is the only frequency sensitive to this parameter. From the comparison of these Jacobians calculated with the three RTMs models, we observe that their largest differences come from the treatment of the OWS.

2.2 Dataset preparation

AMSR2 was launched on 18 May 2012 on board JAXA GCOM-W1, and SMAP was launched on 31 January 2015. Three days (5,15, 25) of the months of January, April, July, and October in 2016 are selected for the analysis. For AMSR2, we use the Top of Atmosphere (TOA) TBs Level L1R provided by the JAXA platform (`https://gportal.jaxa.jp/gpr/`, last access 15/07/2019). Each channel is selected at its own spatial resolution except for the 89 GHz channel which is at the same spatial resolution as the 36.5 GHz channel. For SMAP, we use directly the surface TBs, computed by RSS and provided by NASA Jet Propulsion Laboratory (`https://podaac.jpl.nasa.gov/dataset/SMAP_RSS_L2_SSS_V2`, last access 15/07/2019). These L-band TBs are corrected for the galactic signal, from the Faraday rotation, as well as for atmospheric effects.

The SMAP and AMSR2 observations are collocated with surface and atmospheric parameters from the European Centre for Medium-Range Weather Forecasts (ECMWF) Re-Analysis (ERA)-Interim and from the Mercator Ocean reanalysis (*Global Analysis Forecast Phy 001 024* distributed by the Copernicus Marine Service, Lellouche et al. (2019)). ECMWF ERA-interim at 0.25° is adopted for the atmospheric fields, at different pressure levels. The OWS, the Total Column Water Vapor (TCWV), and the Total Column Liquid Water (TCLW) are also extracted from ERA-interim, but at 0.125°. Both contain reanalysis information at 00:00 06:00 12:00, and 18:00 UTC. The Mercator data at

Figure 1. Jacobians of the ocean surface brightness temperature with respect to SST (top), OWS (middle), and SSS (bottom), as a function of frequency for an incidence angle of 55°. The oceanic conditions are SST = 291 K, OWS = 6 m/s, and SSS = 34 psu. The atmosphere is not considered here.

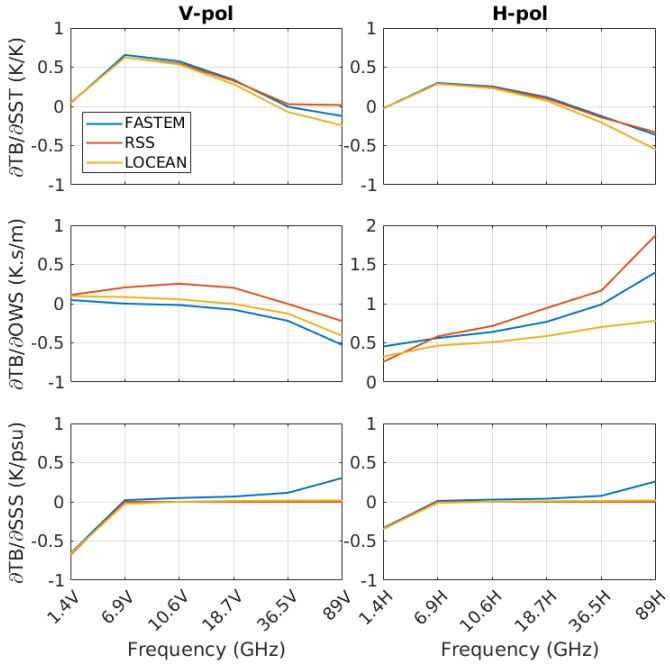

0.083° spatial resolution are selected for SST and SSS. For the SST, the hourly information is extracted and for the SSS the daily averages are used. The collocation with AMSR2 and SMAP data is performed with nearest neighbor interpolation, spatially and temporally. Two different datasets are created: one with AMSR2 TOA TBs collocated with the geophysical parameters, and one with SMAP surface TBs also collocated with the geophysical parameters.

The quality of the data selected as input parameters to the RTMs is also very important, as errors in the input parameters will directly impact the simulated TBs. The accuracy of the Mercator products are documented in Lellouche et al. (2019). The SST has mean error between -1 to +1 K . The SSTs in cold regions tend to be underestimated (up to 1 K) while the SSTs near the equator especially in the Pacific Ocean can be overestimated (up to 0.5 K). The SSS from Mercator data rarely exceeds 0.1 psu. In high variability regions like the Gulf Stream or the Agulhas Current, or the Eastern Tropical Pacific, the SSS error can reach more than 0.5 psu locally (Lellouche et al., 2019). Mercator reanalysis uses the atmospheric fields from ECMWF ERA-Interim, therefore inconsistencies between the selected surface and atmospheric fields should be limited. The OWS from ERA-Interim has been studied by Stopa and Cheung (2014). This study shows that ECMWF OWS are overestimated for the lower wind speeds (around 0.25 m/s) and underestimated for the upper wind speeds (around 1.5 m/s). Zhang et al. (2018) compared wind speed from microwave radiometers (WindSat, SSMI, AMSR-E and AMSR2) with in-situ and ECMWF wind speeds. In comparison with the ECMWF data, positive differences are found at high southern latitudes in January and at high northern latitudes in July.

The selection of the geophysical parameters, as well as the selection of the TBs datasets, can affect the comparison results and one has to be aware of it. The RSS RTM has been

developed using OWS derived from WindSat, QuikSCAT, and SSMIS (Special Sensor Microwave Imager Sounder), and NCEP (National Center for Environmental Prediction) GDAS (Global Data Assimilation System) wind directions, while LOCEAN and FASTEM RTMs have been developed using ECMWF wind speed. On the other hand, the L-band data used in this study comes from the SMAP instrument and has been corrected by RSS, whereas LOCEAN model at L-band has been fine-tuned with SMOS L-band data. For this global and systematic analysis of the different models over a large frequency range, choices had obviously to be made. However, these aspects will be remembered and care will be exercised in the interpretation of the comparison results.

2.3 Methodology

The ocean RTMs (FASTEM, RSS, LOCEAN) are fed with the geophysical parameters to calculate the sea surface emissivity. For SMAP data provided by RSS, we compare directly the sea surface TBs that are already corrected for the atmospheric effects. For AMSR2 data, the atmospheric contribution is simulated with RTTOV version 12 (Saunders et al., 1999, 2018), with inputs from the atmospheric profiles (pressure, temperature, humidity, and liquid water), and the sea surface emissivity to compute the TOA TBs. Moreover, the estimation of a scattering term is needed when computing TOA TBs: it represents the part of the downwelling atmosphere radiation scattered by the ocean surface in the satellite direction and it depends on the atmospheric conditions and sea surface roughness. The computation method can be different according to the RTM. For FASTEM, the scattering term is taken into account as a multiplicative coefficient on the reflectivity of the sea surface. For RSS, it is computed as an additive term to the final TOA TB. For LOCEAN RTM we apply the same scattering term as in the RSS RTM.

To perform the simulation / observations comparison, we filter out the sea ice and the coastal areas at 50 km from the continent. Only cases with TCLW < 0.01 kg.m^{-2} are considered to limit the contamination by clouds, especially at frequencies > 18 GHz. This threshold has been carefully tested to minimize the potential cloud contribution, without suppressing too many cases.

Systematic error between the observations and the simulations are first evaluated. The systematic error (i.e., the bias) is computed as the global mean difference between the observations and the simulations. Thus, after correction of the systematic errors, the difference between the simulations and the observations is centered. In a second step, the precision of the RTMs is estimated as a function of the sea surface parameters.

The observations over the globe are not equally distributed between latitude ranges when using data from a satellite in polar orbit. The observations over the poles are more frequent and the ocean areas are larger at lower latitudes. The high latitude observations (> 60°N and S) represent around 10% of the total number of observations, while the low latitudes (0°-30°N and S) and the mid latitudes (30°-60°N and S) represent both around 45%. This has to be remembered when analyzing the data, and this observation distribution is representative of satellites in polar orbit, often used for oceanic and meteorological applications.

SSTs are between 273 and 305 K with a mode value at 303 K, OWSs are between 0 and 20 m/s (mode value of 7 m/s), and SSSs between 32 and 38 psu (mode value at 35 psu). TCWV distribution is between 2 and 60 kg.m^{-2} (mode value at 5 kg.m^{-2}) and TCLW is between 0 and 0.01 kg.m^{-2}, as higher values have been excluded from the dataset to limit contamination by clouds. The geophysical variables are correlated and interdependent (see Fig. 2). For example, at high latitude regions, TCWV is low, SST is cold, and OWS is in average higher, while at the Equator, TCWV is large, SST is warm, and OWS is lower. These correlations make it difficult to isolate the effect of only one parameter on the observed TBs, and it is important to be aware of the distributions and correlations of the parameters to correctly interpret the results. The highest correlation

Figure 2. Correlation between the geophysical variables estimated from AMSR2 observations.

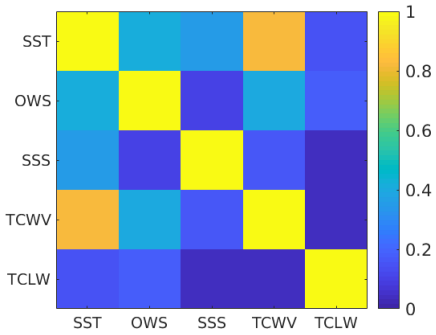

is found between SST and TCWV. Some cases are also rarely observed, such as strong OWS above 15 m/s, or very low SST or SSS. Note that RTMs are usually designed to work better on frequently observed ocean states.

3 Results

3.1 Systematic error estimation

Systematic errors between the TBs observed from SMAP and AMSR2, and the TBs simulated with the different ocean RTMs are first estimated. The mean value of the difference between observed TBs and simulated TBs for each channel is computed considering only the cases with OWS < 7 m/s. Higher OWS were excluded to this calculation as large discrepancies were observed between the observations and the models for these higher wind speeds: it does not change the conclusion of the analysis, it just changes the TB references. Figure 3 shows these systematic errors and their respective Standard Deviations (StDs) for each channel and each ocean RTM. The systematic errors between the observations and the simulations can come from instrument calibration issues, ocean RTMs, ancillary data used as inputs to run the RTMs, or from time or space mismatch between the geophysical parameters and the observations.

Systematic errors between SMAP observations and RTM simulations are < 0.9 K (see Fig. 3). Part of these biases could be related to instrument calibration. Peng et al. (2017) tested the SMAP calibration with respect to SMOS data and found a shift of 0.66 K and 0.21 K respectively for vertical and horizontal polarizations over ocean between the two instruments, which is lower than the biases observed with some simulations. Systematic errors estimated between AMSR2 observations and RTM simulations are much larger than with SMAP. AMSR2 instrument calibration has been studied by Alsweiss et al. (2015) and Okuyama and Imaoka (2015). Using the double difference method, they found biases up to 5 K over ocean between AMSR2 and TMI, depending on the channels. Therefore, AMSR2 and / or TMI instruments have calibration issues. The computed systematic errors differ among the ocean RTMs, evidencing nevertheless important differences between the models.

In operational applications for the analysis of the ocean variables from satellite data, the systematic errors are subtracted. The key information is the variation of the TBs as a function of the oceanic parameters. In the following analysis, the systematic RTM errors are removed and the difference between the observations and the simulations are studied, as a function of the sea surface parameters (SST, OWS, SSS).

Figure 3. Systematic errors between SMAP/AMSR2 observations and the RTM simulations, computed as the mean value of $TB_{observed}$ - $TB_{simulated}$. The systematic errors are represented in solid lines and their Standard Deviations (StDs) are represented in dashed lines.

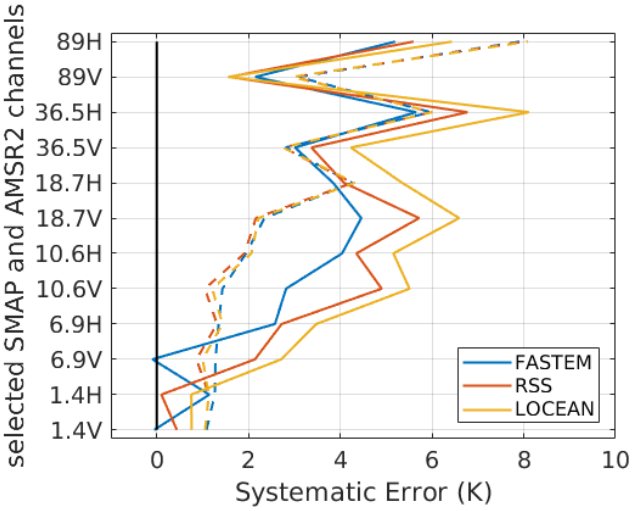

3.2 Evaluation of the simulated brightness temperatures as a function of sea surface parameters

3.2.1 Comparisons of the brightness temperatures

Figures 4 and 5 (top panels) show the observed and simulated TBs (corrected from the systematic errors), as a function of SST for different ranges of OWS, at 1.4 and 6.9 GHz for both orthogonal polarizations. The variability of the signal as a function of SST is small at 1.4 GHz and the differences between the observations and the RTM simulations are limited. At 1.4 GHz, LOCEAN and RSS RTMs are close to the SMAP observations. FASTEM differs more from the observations, especially at horizontal polarization and for strong OWS: this is expected as FASTEM has not been developed for applications at L-band. At 6.9 GHz, the TBs increase quasi-linearly with the SST, making this frequency particularly suitable for the analysis of the SST. At 6.9 GHz and higher frequencies (not shown here), LOCEAN RTM is closer to the AMSR2 observations at low OWS especially for cold water, as compared to the other RTMs. The sensitivity to SST for cold SST (270-280 K) is not well represented with FASTEM and RSS RTMs. This shows that there is not one perfect RTM, regardless of frequencies and sea surface parameters.

Similarly to the previous figures but as a function of the OWS and for different SSTs, Figures 4 and 5 (bottom panels) show the observed and simulated TBs (corrected from the systematic errors), at 1.4 and 6.9 GHz for both orthogonal polarizations. At 1.4 GHz, the variability of the TB as a function of OWS is well represented with LOCEAN and RSS RTMs. At 1.4 GHz, FASTEM fails to represent the correct sensitivity for OWS $>$ 12 m/s. At frequencies from 6.9 to 36.5 GHz (not shown), FASTEM and LOCEAN RTMs underestimate the TB for OWS $>$ 7 m/s. RSS RTM agrees reasonably well with the observations as a function of OWS. The RSS parametrization used to describe the OWS sensitivity is different at 1.4 GHz than at higher frequencies (6.9 to 89 GHz). The LOCEAN RTM fits well the observations at 1.4 GHz but does not at high wind speeds at higher frequencies: this shows some deficiency in the treatment of the OWS dependence at higher frequency, coming from the roughness model and/or from the foam treatment. The same is observed for FASTEM with an acceptable OWS dependence up to 12 m/s at 1.4 GHz and only up to 7 m/s at higher frequencies.

Figure 4. TB comparisons between observations and RTM simulations at 1.4 GHz at vertical (left) and horizontal (right) polarizations. In the top panels the TBs are plotted as a function of SST for different ranges of OWS (colors). In the bottom panels the TBs are plotted as a function of OWS (bottom) for different ranges of SST (colors). The SSS range is between 34 and 36 psu.

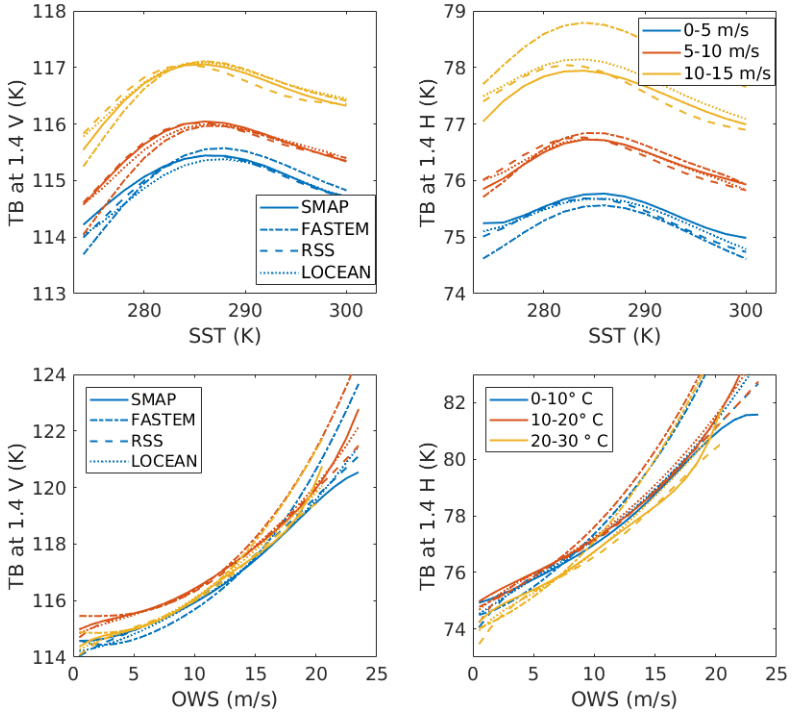

Figure 5. TB comparisons between observations and RTM simulations at 6.9 GHz at vertical (left) and horizontal (right) polarizations. In the top panels the TBs are plotted as a function of SST for different ranges of OWS (colors). In the bottom panels the TBs are plotted as a function of OWS for different ranges of SST (colors). The TCWV range is between 0 and 15 kg.m^{-2}.

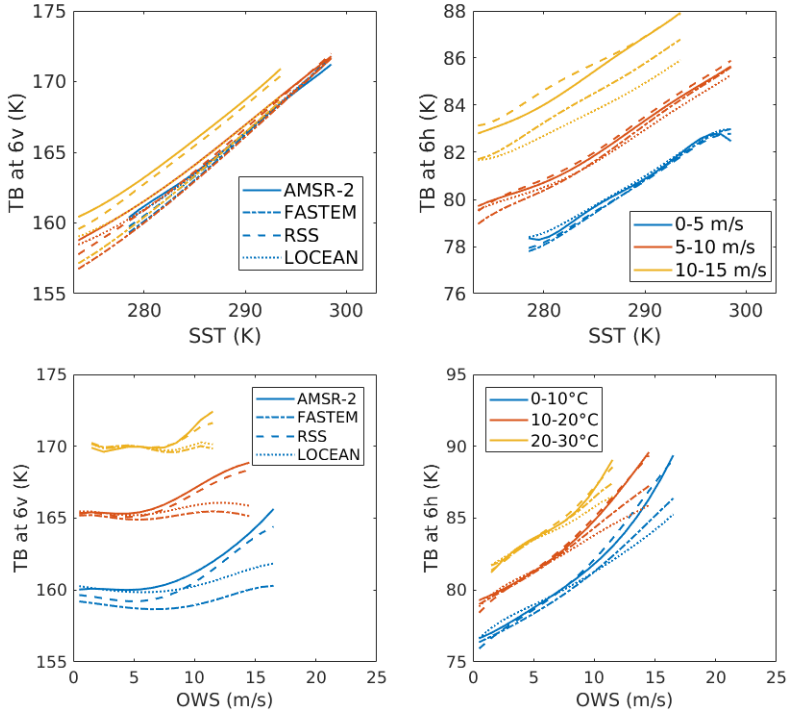

Figure 6. Difference between the SMAP surface TB observations and the RTM simulations (corrected for the systematic errors) at 1.4 GHz as a function of OWS (left panel), SST (middle panel), and SSS (right panel). For comparisons as a function of SST and SSS, only observations with OWS < 7 m/s are taken into account. The distribution of the number of observations as a function of the sea surface parameters (OWS, SST, SSS) are represented in grey bars with legend in right y-axis.

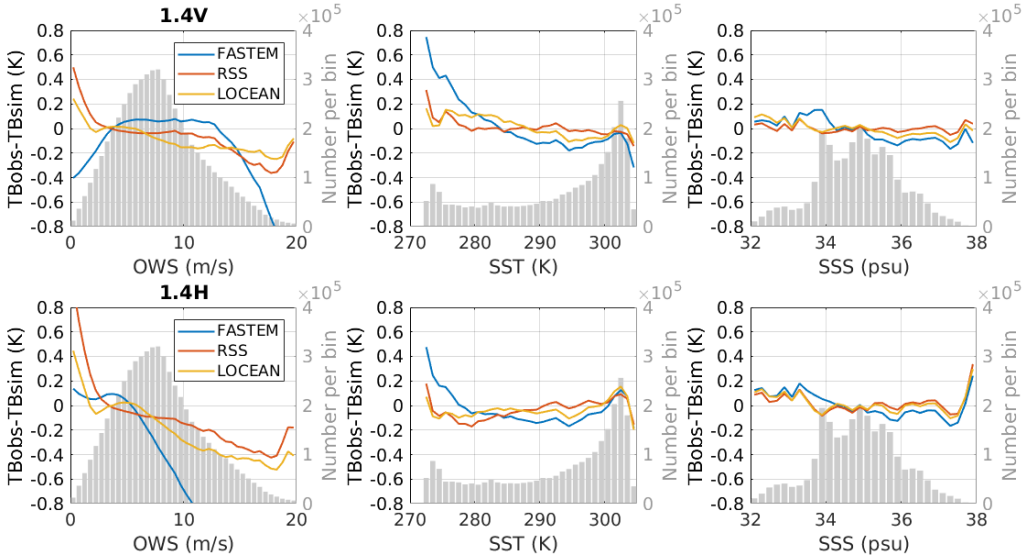

3.2.2 Analysis of the differences between observed and simulated brightness temperatures

We now focus on the ability of the different RTMs to correctly reproduce the TB variability according to the different sea surface parameters (SST, SSS, OWS). For all considered frequencies, Figures 6 to 11 present the comparison between SMAP or AMSR2 TBs with the TBs simulated with FASTEM, RSS, and LOCEAN RTMs as a function of SST, SSS, and OWS. For the analysis of SST and SSS dependences, only the cases where OWS is less than 7 m/s are considered, to avoid the large and possibly misleading errors introduced when OWS is strong.

At 1.4 GHz, RSS and LOCEAN simulations are in good agreement with the observations (see Fig. 6). The variability of the TBs as a function of SST, SSS, and OWS is correctly simulated, as the differences between the simulated and the observed TBs are rather stable. For FASTEM at 1.4 GHz, the TBs are overestimated for OWS > 12 m.s^{-1}. For cold SST, the errors at 1.4 GHz are larger. At very low OWS (0-2 m/s) there are also larger errors. The ocean surface can actually be rough even at very low OWS, due to the swell which is not taken into account in the RTMs here. At horizontal polarization, the OWS dependence is less well represented than at vertical polarization. For the comparison with SMAP observations, the RSS model is advantaged, as the SMAP TB surface observations used in this study are generated by RSS.

At frequencies above 1.4 GHz (see Fig. 7 to 11), the OWS dependence is not correctly simulated with FASTEM (as already observed by Bormann et al. (2012)) or with LOCEAN model for high wind speeds: the TBs are underestimated at OWS > 7 m/s. To describe the OWS dependence, LOCEAN model and FASTEM use 3 components: a roughness model, a foam coverage, and a foam emissivity, whereas the RSS model uses a parametrization of the OWS dependence based directly on observations, from Aquarius at 1.4 GHz and from SSMI and WindSat at frequencies between 6.9 and 89 GHz. For

Figure 7. Difference between the AMSR2 top of atmosphere TB observations and the RTM simulations (corrected for the systematic errors) at 6.9 GHz as a function of OWS (left panel), SST (middle panel), and SSS (right panel). For comparisons as a function of SST and SSS, only observations with OWS < 7 m/s are taken into account. The distribution of the number of observations as a function of the sea surface parameters (OWS, SST, SSS) are represented in grey bars with legend in right y-axis.

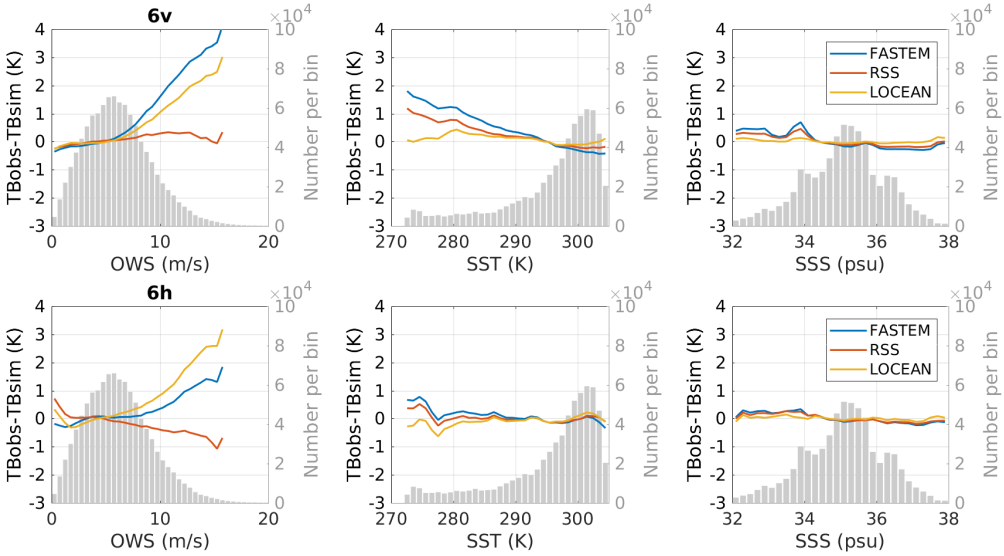

Figure 8. Same as Figure 7 at 10.65 GHz.

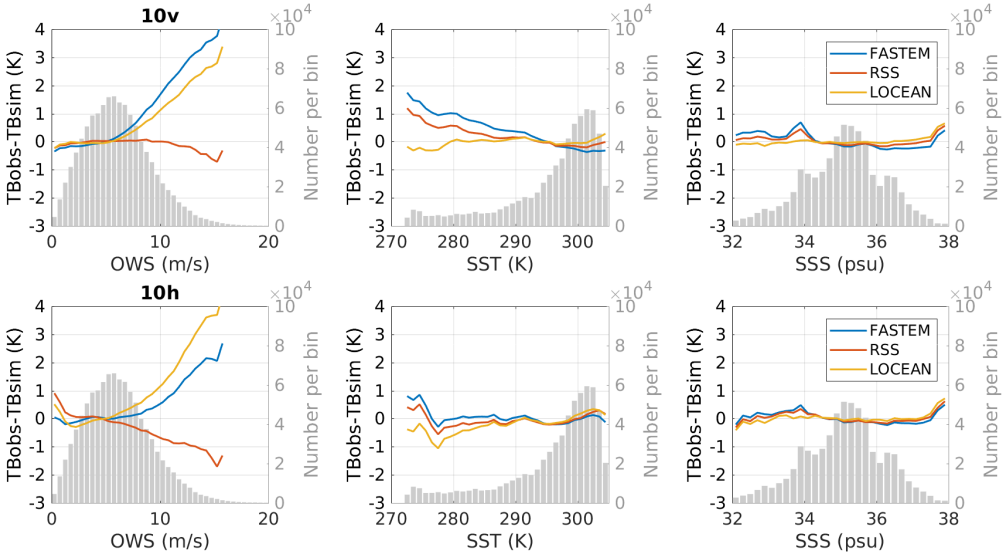

Figure 9. Same as Figure 7 at 18.7 GHz.

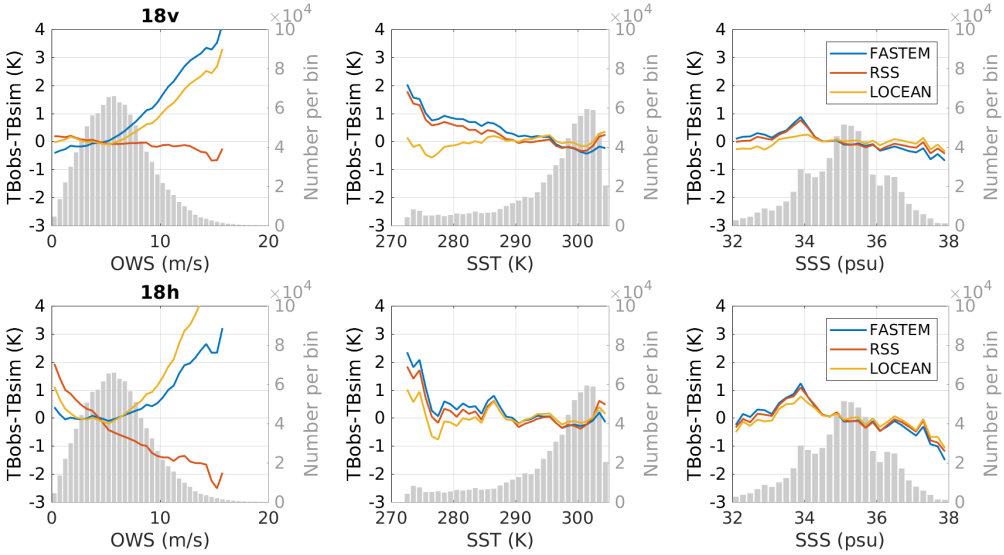

Figure 10. Same as Figure 7 at 36.5 GHz.

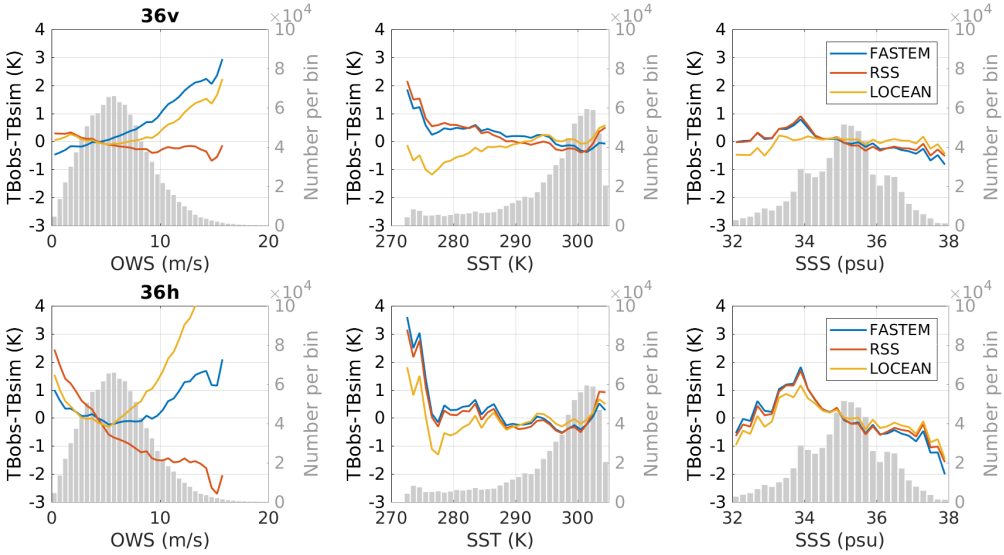

Figure 11. Same as Figure 7 at 89 GHz.

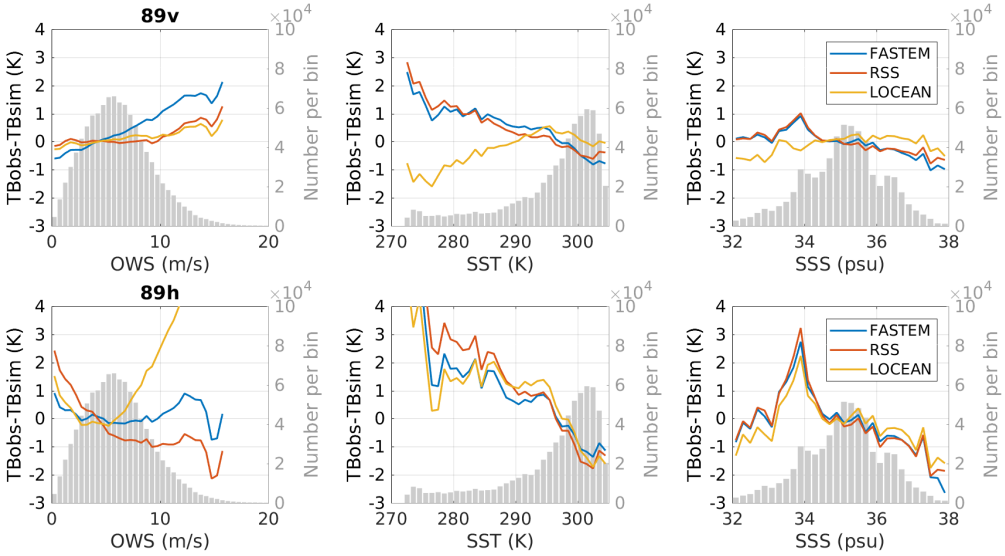

the RSS RTM, the difference with the observations are lower than 1 K up to 10.65 GHz. At higher frequencies in horizontal polarization, the differences between simulations and observations are larger. At these frequencies and especially for the horizontal polarization, the sensitivity to water vapor and liquid water is larger: uncertainties in the atmospheric RTM and in the ancillary atmospheric fields can also introduce errors in the results, despite the filtering of most cloudy scenes.

The analysis of the SSS dependence shows that the discrepancy between simulations and observations increases with decreasing SSTs. For cold waters, the models tend to show large differences with the observations (especially FASTEM). The possible contamination of the observations with sea ice has been carefully examined, and eliminated as much as possible. Note that the difference between LOCEAN and the observations has often the opposite sign that the two other models. For frequencies above 18 GHz in horizontal polarization, all RTM simulations disagree with the observations for the low SSTs. These frequencies and polarization are more sensitive to the atmospheric parameters but the reason of the increased discrepancy is not clear at that stage.

For large SST above 303 K, a peak in the absolute differences with the observations is observed for all RTMs above 10 GHz, especially in the horizontal polarization. It is explained by the strong correlation between the large SSTs and the high TCWVs, typically in tropical areas. The tropical atmosphere is saturated with water vapor. First, uncertainty in the water vapor content and modeling can introduce additional errors. Second, the probability of clouds increases in these atmospheres, and they are not necessarily well characterized in the ECMWF reanalysis (Geer et al., 2017).

For the SSS dependence, the differences between observations and RTM simulations are limited, even at 1.4 GHz despite its high sensitivity to this parameter. This is rather encouraging as this is the key frequency for the analysis of the SSS from satellites. Note that the increase of the errors at SSS close to 38 psu in horizontal polarization at 1.4 GHz is associated to a very limited number of observations and should be considered with caution (see the related histograms of occurence). At frequencies above 1.4 GHz, the sensitivity to the SSS is very limited (Figure 1). Small changes in the differences as a function of SSS are likely due to correlation with other parameters (SST or OWS).

4 Discussion

4.1 Dielectric Constant

The sensitivity of the sea surface emissivity to SST and SSS is related to the dielectric constant module of the ocean RTMs. In the previous section, we observed that the TB for cold SST is underestimated with the RSS and FASTEM RTMs between 6.9 and 89 GHz, and mostly overestimated with LOCEAN RTM above 10 GHz. From 6.9 GHz to 10.6 GHz at vertical polarization, the LOCEAN RTM with the dielectric constant of Klein and Swift (1977) is closer to the observations than FASTEM or RSS RTMs using, respectively, Liu et al. (2011) and Meissner and Wentz (2012) dielectric constants. With increasing frequencies, LOCEAN results degrade as the Klein and Swift (1977) dielectric constant model is supposed to be valid only for low frequencies with its simple Debye formula. The models of Liu et al. (2011), and of Meissner and Wentz (2012) use a double Debye formula and should be more appropriate at higher frequencies.

SST strongly correlates with water vapor, and at higher frequencies (18-89 GHz) the contribution of the atmospheric attenuation by water vapor strongly increases. Therefore, the SST dependent biases in Figures 9-11 could also be caused by imperfections in the atmospheric vapor absorption model or the vapor input rather than the dielectric constant model. The combination of the TBs : $2 \times TB_{V-pol} - TB_{H-pol}$ is less sensitive to errors in the atmospheric absorption than the single V-pol and H-pol channels are Meissner and Wentz (2002). When simulating this combination and comparing it to observations (not shown here), the differences do not change much with SST. This indicates, that the observed biases in the FASTEM and RSS at the higher frequencies in Figures 9-11 are likely due to issues with the water vapor absorption and not with the dielectric constant model.

The dielectric constant module of the ocean RTMs can be changed to better fit the observations. The difficulty is to develop an accurate dielectric constant model over a large range of parameters (frequency, angle, SST, SSS). Lawrence et al. (2017) tested FASTEM with a range of measurements for the dielectric constant, and compared the simulated TBs to satellite observations, with the objective of detecting SST dependent biases that could indicate errors in the dielectric constant model for seawater. Their results also plead for reference quality measurements of the dielectric constants, covering the large variability of the different parameters, and including uncertainty estimates. Lang et al. (2016); Zhou et al. (2017) initiated such efforts at 1.4 GHz, but it should be extended to higher frequencies, especially at 6 GHz which is the preferred frequency for SST analysis.

4.2 Foam and roughness models

Errors in the OWS dependence of LOCEAN and FASTEM RTMs are evidenced in Section 3. They can come from three different components of the models. To increase the simulated TB with increasing OWS, there are different possibilities: (1) increase the foam emissivity (noting that it is already close to one, except for L-band), (2) modify the foam coverage model, or (3) modify the roughness model. The key input of the roughness model is the wave spectrum. Different combinations of foam coverages, foam emissivities, and wave spectra are tested to analyze how these terms impact the simulated TBs.

Foam cover models such as Tang (1974), Wu (1979) or Monahan and O'Muircheartaigh (1980) lead to an overestimation of the sea surface emissivity at high OWS. Other foam coverage models such as Monahan and O'Muircheartaigh (1986), Yin et al. (2012) or Yin et al. (2016) tend to underestimate the sea surface emissivity above 1.4 GHz. M. D. Anguelova and Webster (2006) show that the foam coverage in the microwaves is underestimated using data from photos or video as it detects only the bright active whitecap and does not reveal the aged whitecap that is less bright. M. D. Anguelova and Webster (2006)

developed a foam cover dataset derived from satellite microwave observations and found two different foam coverages at 10 and 37 GHz. The foam coverage, or more precisely the fraction of foam which impacts the signal at a given frequency, increases with the frequency. At low microwave frequencies (e.g., 1.4 GHz), the penetration depth is expected to be larger, meaning that only thick foam layers are detected. With increasing frequency, the penetration depth decreases and the signal becomes sensitive to thiner foam layers. Therefore, at higher frequencies (e.g., 37 GHz) the signal is sensitive to a larger range of foam thicknesses, and the effective foam coverage increases. Based on the M. D. Anguelova and Webster (2006) datasets, Salisbury et al. (2013) and Albert et al. (2016) proposed foam cover models for selected frequencies (see Figure 12, left). Meunier et al. (2014) and M. Anguelova et al. (2014) suggested the possibility of deriving the foam coverage from wave dissipative energy calculated from a wave model: this possibility will have to be further investigated.

The foam emissivity model also has an impact on the total foam signal. The foam emissivity is generally close to 1 for the microwaves between 6 and 90 GHz (e.g., Kazumori et al. (2008) and Liu et al. (2011)), whereas it is lower for the L-band RTM (Yin et al., 2016). Stogryn (1972) already introduced a dependence with the frequency but it cannot be applied at frequencies > 60 GHz (see Figure 12, right). More recently, M. D. Anguelova and Gaiser (2013) suggested a foam emissivity model taking into account the foam thickness and depending on the frequency. For a given thickness, the emissivity increases with frequencies (see Figure 12, right).

In Figure 13, the RTM results are tested with different combinations of foam cover and foam emissivity models. The RSS model is taken as the reference as it shows the best results in terms of TB variability with OWS. FASTEM RTM is tested with the original foam cover of version 5 (Monahan & O'Muircheartaigh, 1986), with the foam cover of version 4 (Tang, 1974), as well as without any foam cover: it clearly underlines the impact of the foam model on the results. For the LOCEAN RTM, we tried several combinations of foam coverage and emissivity models, with the objective of fitting the observations as well as possible from 1.4 to 37 GHz. The Albert et al. (2016) model at 37 GHz predicts large foam cover for intermediate wind speeds (Figure 12, left). To simulate the dependence with the frequency, the foam emissivity model of M. D. Anguelova and Gaiser (2013) is tested with different foam thicknesses (as shown in Yin et al. (2016)) to obtain the maximum emissivity at 37 GHz, and the appropriate emissivities at lower frequencies. Associated to the foam emissivity of M. D. Anguelova and Gaiser (2013) (with a thickness of 2 mm), a reasonable agreement is obtained between model and observations at 1.4 and 6 GHz. Future work will be necessary to refine the combination of foam cover and emissivity, with sound physical basis (e.g., a foam thickness distribution instead of a foam cover).

The wave spectrum influence can be studied only with the LOCEAN physical model, as RSS and FASTEM RTMs are parameterized. Dinnat et al. (2003) and Yin et al. (2016) already tested different wave spectrum models such as Elfouhaily et al. (1997), Kudryavtsev et al. (1999), and Durden and Vesecky (1985). They chose the model of Durden and Vesecky (1985) and optimized it to L-band observations by multiplying the spectrum amplitude coefficient of Durden and Vesecky (1985) by 1.25. For its double-scale ocean RTM, Yueh (1997) used the model of Durden and Vesecky (1985) and multiplied the amplitude coefficient by 2 (referenced as DV2 in the figures): it results in a twice larger slope and height variances of the waves. Figure 13 shows some tests and illustrates the impact of the wave spectrum on the LOCEAN model at 1.4 and 6.9 GHz. By multiplying the wave spectrum amplitude coefficient of Durden and Vesecky (1985) by 2 compared to 1.25, we can observe that at 1.4 GHz the emissivities at medium and strong OWS are overestimated, and at 6.9 GHz in vertical polarization the emssivities at strong OWS are still underestimated, while in horizontal polarization at low OWS the emssivities are overestimated.

Figure 12. Comparison of the foam coverage models as a function of OWS (left) and comparison of foam emissivity models as a function of frequency (with t the foam thickness) (right).

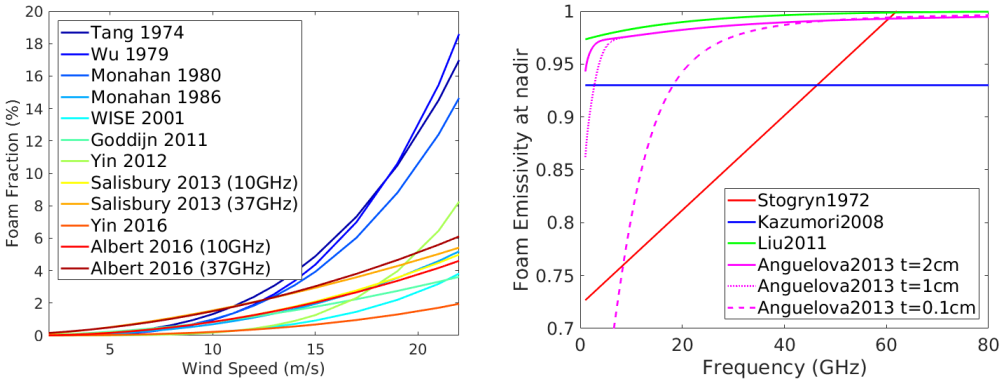

Figure 13. Brightness temperature at 1.4 GHz and 40^o incidence angle (top) and at 6.9 GHz and 55^o incidence angle (bottom) as a function of OWS, for different combinations of wave spectrum, foam cover, and foam emissivity models. DV2 refers to the wave spectrum of Durden and Vesecky (1985) (DV) with the amplitude coefficient multiplied by 2. t is the foam thickness in the model of M. D. Anguelova and Gaiser (2013).

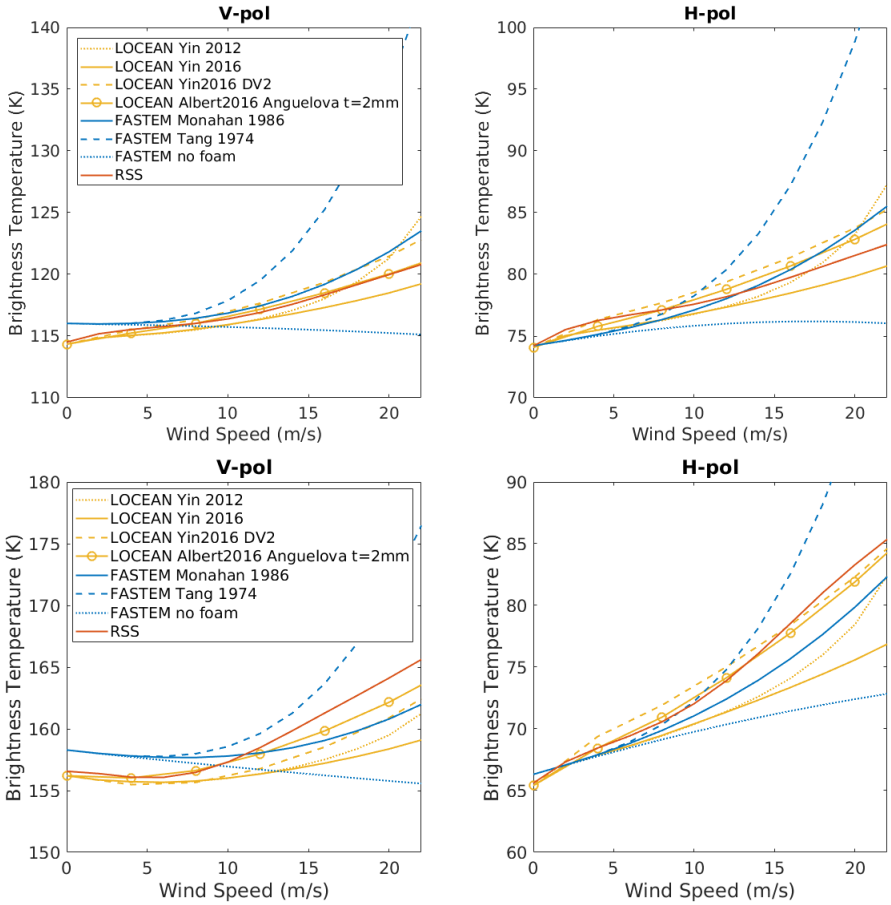

5 Conclusion

Three ocean emissivity models have been compared with satellite observations from 1.4 GHz to 89 GHz. They are representative of the three classes of models: LOCEAN a physical model with parameters adjusted to L-band, FASTEM a fast parameterized model, and RSS an empirical model fitting satellite observations. This comparison exercise was based on a dataset of satellite observations from SMAP and AMSR2, collocated with surface and atmospheric parameters from ECMWF ERA-Interim and Mercator reanalysis data. The database samples the global ocean over a year. The TBs were simulated for the three ocean emissivity RTMs, adding the atmospheric contribution calculated from RTTOV when needed.

The simulations were carefully compared to the observed TBs. Firstly, global systematic errors between simulations and observations were computed. The biases tend to increase with frequency, and are generally higher at horizontal than at vertical polarizations. This is partly due to the increasing effect of the atmospheric contribution with frequency (essentially undetected clouds), especially at horizontal polarization. Part of it can also stem from AMSR2 calibration issues. Secondly, the analysis focussed on the accuracy of the RTMs as a function of the key ocean variables, SST, SSS, and OWS (once the global biases are subtracted).

Major discrepancies with the observations were found at frequencies above 1.4 GHz, for OWS higher than ~ 7 m/s, with the LOCEAN and the FASTEM models, with differences strongly increasing with increasing OWS. Possible model improvements were discussed. The analysis tended to show that a frequency dependence needs to be added to the foam cover model or / and to the foam emissivity model. The study also stressed that these two components have to be considered consistently and jointly, all over the frequency range. Efforts should be devoted to the modeling of the foam contribution, taking into account the OWS, but also the frequency dependence, and possibly the wave dissipative energy, as already suggested by Reul and Chapron (2003), Meunier et al. (2014), and M. Anguelova et al. (2014).

Cold SSTs were identified as a source of disagreement between the simulations and the observations, regardless of the model. This is a critical issue, especially at vertical polarization at 6 GHz which is the key channel for the SST analysis from satellites. Larger uncertainties at cold SST are partly due to uncertainties in the modeling of the dielectric constants of sea water, but they can also come from inaccuraccy in the reanalisys data or due to high wind speed effects in cold regions. New laboratory measurements of the dielectric properties of ocean water have recently been undertaken at 1.4 GHz (Lang et al., 2016; Zhou et al., 2017): their extension to a larger range of SST and SSS at higher frequencies should be encouraged, insisting on the uncertainty estimation and with special attention to the 6 GHz.

Here, observations from the conical imagers SMAP and AMSR2 have been analyzed, at fixed incidence angles. Observations from the Global Precipitation Mission (GPM) Microwave Instrument (GMI), from 10 to 190 GHz, should be considered soon as this instrument has been shown to be very well calibrated. Future work will also study the angular dependence of the emission signal with observations from the sounders such as the Advanced Microwave Sounding Unit - A (AMSU-A) that measure with incidence angles from nadir up to 60°.

New mission projects such as the Copernicus Imaging Microwave Radiometer (CIMR) (Kilic et al., 2018) requires the development of consistent and accurate ocean surface emissivity models over a large frequency range (here from 1.4 to 36 GHz). More generally, the lack of a reference quality ocean emission model in the microwaves has already been identified at several occasions by the international community (`https://www.jcsda.noaa.gov/meetings_JointEC-JC_Wkshp2015_agenda.php,http://cimss.ssec.wisc.edu/`

551 itwg/itsc/itsc21/). The present study identified major issues in the current models.
552 It is the first step toward the development of a new physically-based community model
553 to provide consistent results over the microwave range currently (or soon-to-be) observed
554 from satellites and for all the observing conditions.

555 **Acknowledgments**

556 AMSR2 data are available at https://gportal.jaxa.jp/gpr/ (last access 15/07/2019),
557 SMAP data are available at https://podaac.jpl.nasa.gov/dataset/SMAP_RSS_L2_SSS
558 _V2 (last access 15/07/2019), ECMWF reanalysis data are available at https://apps
559 .ecmwf.int/datasets/data/interim-full-daily/levtype=sfc/ (last access 15/07/2019)
560 and Mercator Ocean reanalysis data are available at http://marine.copernicus.eu/
561 services-portfolio/access-to-products/?option=com_csw&view=details&product
562 _id=GLOBAL_ANALYSIS_FORECAST_PHY_001_024 (last access 15/07/2019). This work has
563 been supported by the Programme National de Télédétection Spatiale (PNTS), http://
564 www.insu.cnrs.fr/pnts grant N° PNTS-2017-08 and the Terre, Océan, Surfaces Con-
565 tinentales, Atmosphère (TOSCA) ocean program from the CNES (Centre National d'Études
566 Spatiales).

567 ## References

568 Albert, M. F., Anguelova, M. D., Manders, A. M., Schaap, M., & De Leeuw, G.
569 (2016). Parameterization of oceanic whitecap fraction based on satellite obser-
570 vations. *Atmospheric Chemistry and Physics*.

571 Alsweiss, S. O., Jelenak, Z., Chang, P. S., Park, J. D., & Meyers, P. (2015). Inter-
572 calibration results of the advanced microwave scanning radiometer-2 over
573 ocean. *IEEE Journal of selected topics in applied earth observations and re-*
574 *mote sensing*, *8*(9), 4230–4238.

575 Anguelova, M., Meunier, L.-F., Bettenhausen, M., Janssen, P., & English, S.
576 (2014). *Validation of foam coverage derived from wave dissipative energy*
577 *from a wave model for rttov* (Tech. Rep. No. NWPSAF-EC-VS-05). EU-
578 METSAT. Retrieved from https://nwpsaf.eu/publications/vs_reports/
579 nwpsaf-ec-vs-025.pdf

580 Anguelova, M. D., & Gaiser, P. W. (2013). Microwave emissivity of sea foam lay-
581 ers with vertically inhomogeneous dielectric properties. *Remote Sens. Environ.*,
582 *139*, 81–96.

583 Anguelova, M. D., & Webster, F. (2006). Whitecap coverage from satellite measure-
584 ments: A first step toward modeling the variability of oceanic whitecaps. *J.*
585 *Geophys. Res.*, *111*(C3), C03017.

586 Atlas, R., Hoffman, R. N., Ardizzone, J., Leidner, S. M., Jusem, J. C., Smith, D. K.,
587 & Gombos, D. (2011). A cross-calibrated, multiplatform ocean surface wind
588 velocity product for meteorological and oceanographic applications. *Bulletin of*
589 *the American Meteorological Society*, *92*(2), 157–174.

590 Bell, M. J., Forbes, R. M., & Hines, A. (2000). Assessment of the foam global data
591 assimilation system for real-time operational ocean forecasting. *Journal of Ma-*
592 *rine Systems*, *25*(1), 1–22.

593 Bormann, N., Geer, A., & English, S. (2012). *Evaluation of the microwave ocean*
594 *surface emmisivity model fastem-5 in the ifs.* European Centre for Medium-
595 Range Weather Forecasts.

596 Carmack, E. C., Yamamoto-Kawai, M., Haine, T. W., Bacon, S., Bluhm, B. A.,
597 Lique, C., ... others (2016). Freshwater and its role in the arctic marine
598 system: Sources, disposition, storage, export, and physical and biogeochemical
599 consequences in the arctic and global oceans. *Journal of Geophysical Research:*
600 *Biogeosciences*, *121*(3), 675–717.

601 Chelton, D. B., & Wentz, F. J. (2005). Global microwave satellite observations of

sea surface temperature for numerical weather prediction and climate research. *Bulletin of the American Meteorological Society*, *86*(8), 1097–1116.

Debye, P. (1929). *Polar molecules,*. New York: The Chemical Catalog Company Inc.

Dinnat, E. P., Boutin, J., Caudal, G., & Etcheto, J. (2003, aug). Issues concerning the sea emissivity modeling at L band for retrieving surface salinity. *Radio Science*, *38*(4).

Durden, S. L., & Vesecky, J. F. (1985). A Physical Radar Cross-Section Model for a Wind-Driven Sea with Swell. *IEEE J. Ocean. Eng.*, *10*(4), 445–451.

Elfouhaily, T., Chapron, B., Katsaros, K., & Vandemark, D. (1997, jul). A Unified Directional Spectrum for Long and Short Wind-Driven Waves. *J. Geophys. Res.*, *102*(C7), 15781–15796.

Ellison, W., Balana, A., Delbos, G., Lamkaouchi, K., Eymard, L., Guillou, C., & Prigent, C. (1998). New permittivity measurements of seawater. *Radio science*, *33*(3), 639–648.

English, S. J., & Hewison, T. J. (1998). Fast generic millimeter-wave emissivity model. In *Microwave remote sensing of the atmosphere and environment* (Vol. 3503, pp. 288–301).

Fore, A. G., Yueh, S. H., Tang, W., Stiles, B. W., & Hayashi, A. K. (2016). Combined active/passive retrievals of ocean vector wind and sea surface salinity with smap. *IEEE Transactions on Geoscience and Remote Sensing*, *54*(12), 7396–7404.

Geer, A., Ahlgrimm, M., Bechtold, P., Bonavita, M., Bormann, N., English, S., ... others (2017). *Assimilating observations sensitive to cloud and precipitation* (Tech. Rep. No. tech. memo. 815). European Centre for Medium-Range Weather Forecasts.

Gentemann, C. L., & Hilburn, K. A. (2015). In situ validation of sea surface temperatures from the gcom-w1 amsr2 rss calibrated brightness temperatures. *Journal of Geophysical Research: Oceans*, *120*(5), 3567–3585.

Imaoka, K., Kachi, M., Kasahara, M., Ito, N., Nakagawa, K., & Oki, T. (2010). Instrument performance and calibration of amsr-e and amsr2. *International Archives of the Photogrammetry, Remote Sensing and Spatial Information Science*, *38*(8), 13–18.

Kazumori, M., Liu, Q., Treadon, R., & Derber, J. C. (2008, feb). Impact Study of AMSR-E Radiances in the NCEP Global Data Assimilation System. *Mon. Weather Rev.*, *136*(2), 541–559.

Kerr, Y. H., Waldteufel, P., Wigneron, J.-P., Delwart, S., Cabot, F., Boutin, J., ... others (2010). The smos mission: New tool for monitoring key elements ofthe global water cycle. *Proceedings of the IEEE*, *98*(5), 666–687.

Kilic, L., Prigent, C., Aires, F., Boutin, J., Heygster, G., Tonboe, R. T., ... Donlon, C. (2018). Expected performances of the copernicus imaging microwave radiometer (cimr) for an all-weather and high spatial resolution estimation of ocean and sea ice parameters. *Journal of Geophysical Research: Oceans*, *123*(10), 7564–7580.

Klein, L., & Swift, C. (1977). An improved model for the dielectric constant of sea water at microwave frequencies. *Oceanic Engineering, IEEE Journal of*, *2*(1), 104–111.

Kudryavtsev, V. N., Makin, V. K., & Chapron, B. (1999, apr). Coupled sea surface-atmosphere model: 2. Spectrum of short wind waves. *J. Geophys. Res. Ocean.*, *104*(C4), 7625–7639.

Lagerloef, G., Colomb, F. R., Le Vine, D., Wentz, F., Yueh, S., Ruf, C., ... others (2008). The aquarius/sac-d mission: Designed to meet the salinity remote-sensing challenge. *Oceanography*, *21*(1), 68–81.

Lang, R., Zhou, Y., Utku, C., & Le Vine, D. (2016). Accurate measurements of the dielectric constant of seawater at l band. *Radio Science*, *51*(1), 2–24.

Lawrence, H., Bormann, N., Geer, A., & English, S. (2017). Uncertainties in the dielectric constant model for seawater in fastem and implications for the cal/val of new microwave instruments. In *Itsc 21 conference proceedings.*

Lellouche, J.-M., Legalloudec, O., Regnier, C., Levier, B., Greiner, E., & Drevillon, M. (2019). *Quality information document for global sea physical analysis and forecasting product global analysis forecast phy 001 024* (Tech. Rep. No. Issue: 2.1). EU Copernicus Marine Service. Retrieved from `http://cmems-resources.cls.fr/documents/QUID/CMEMS-GLO-QUID-001-024.pdf`

Liu, Q., Weng, F., & English, S. J. (2011). An improved fast microwave water emissivity model. *IEEE Transactions on Geoscience and Remote Sensing*, *49*(4), 1238–1250.

Martin, M., Hines, A., & Bell, M. (2007). Data assimilation in the foam operational short-range ocean forecasting system: A description of the scheme and its impact. *Quarterly journal of the royal meteorological Society*, *133*(625), 981–995.

Meissner, T., & Wentz, F. (2002). An updated analysis of the ocean surface wind direction signal in passive microwave brightness temperatures. *IEEE Transactions on Geoscience and Remote Sensing*, *40*(6), 1230–1240.

Meissner, T., & Wentz, F. (2004, sep). The complex dielectric constant of pure and sea water from microwave satellite observations. *IEEE Trans. Geosci. Remote Sens.*, *42*(9), 1836–1849.

Meissner, T., Wentz, F., & Le Vine, D. (2018). The salinity retrieval algorithms for the nasa aquarius version 5 and smap version 3 releases. *Remote Sensing*, *10*(7), 1121.

Meissner, T., & Wentz, F. J. (2012, aug). The Emissivity of the Ocean Surface Between 6 and 90 GHz Over a Large Range of Wind Speeds and Earth Incidence Angles. *IEEE Trans. Geosci. Remote Sens.*, *50*(8), 3004–3026.

Meissner, T., Wentz, F. J., & Ricciardulli, L. (2014). The emission and scattering of l-band microwave radiation from rough ocean surfaces and wind speed measurements from the aquarius sensor. *Journal of Geophysical Research: Oceans*, *119*(9), 6499–6522.

Meunier, L.-F., English, S., & Janssen, P. (2014). *Improved ocean emissivity modelling for assimilation of microwave imagers using foam coverage derived from a wave model* (Tech. Rep. No. NWPSAF-MO-VS-049). EUMETSAT. Retrieved from `https://nwpsaf.eu/publications/vs_reports/nwpsaf-ec-vs-024.pdf`

Monahan, E. C., & O'Muircheartaigh, I. (1980, dec). Optimal Power-Law Description of Oceanic Whitecap Coverage Dependence on Wind Speed. *J. Phys. Oceanogr.*, *10*(12), 2094–2099.

Monahan, E. C., & O'Muircheartaigh, I. G. (1986, may). Whitecaps and the passive remote sensing of the ocean surface. *Int. J. Remote Sens.*, *7*(5), 627–642.

Monaldo, F. M., Li, X., Pichel, W. G., & Jackson, C. R. (2014). Ocean wind speed climatology from spaceborne sar imagery. *Bulletin of the American Meteorological Society*, *95*(4), 565–569.

Okuyama, A., & Imaoka, K. (2015). Intercalibration of advanced microwave scanning radiometer-2 (amsr2) brightness temperature. *IEEE Transactions on Geoscience and Remote Sensing*, *53*(8), 4568–4577.

Peng, J., Misra, S., Piepmeier, J. R., Dinnat, E. P., Hudson, D., Vine, D. M. L., ... Jackson, T. J. (2017, Sept). Soil moisture active/passive l-band microwave radiometer postlaunch calibration. *IEEE Transactions on Geoscience and Remote Sensing*, *55*(9), 5339-5354. doi: 10.1109/TGRS.2017.2705342

Reul, N., & Chapron, B. (2003). A model of sea-foam thickness distribution for passive microwave remote sensing applications. *Journal of Geophysical Research: Oceans*, *108*(C10).

Reul, N., Fournier, S., Boutin, J., Hernandez, O., Maes, C., Chapron, B., ... others

(2014). Sea surface salinity observations from space with the smos satellite: A new means to monitor the marine branch of the water cycle. *Surveys in Geophysics*, *35*(3), 681–722.

Salisbury, D. J., Anguelova, M. D., & Brooks, I. M. (2013). On the variability of whitecap fraction using satellite-based observations. *Journal of Geophysical Research: Oceans*, *118*(11), 6201–6222.

Saunders, R., Hocking, J., Turner, E., Rayer, P., Rundle, D., Brunel, P., ... Geer, A. (2018). An update on the rttov fast radiative transfer model (currently at version 12). *Geoscientific Model Development*, *11*(7), 2717–2737.

Saunders, R., Matricardi, M., & Brunel, P. (1999). *A fast radiative transfer model for assimilation of satellite radiance observations-rttov-5.* ECMWF Reading, UK.

Stogryn, A. (1972). The emissivity of sea foam at microwave frequencies. *Journal of Geophysical Research*, *77*(9), 1658–1666.

Stopa, J. E., & Cheung, K. F. (2014). Intercomparison of wind and wave data from the ecmwf reanalysis interim and the ncep climate forecast system reanalysis. *Ocean Modelling*, *75*, 65–83.

Tang, C. C. H. (1974, oct). The Effect of Droplets in the Air-Sea Transition Zone on the Sea Brightness Temperature. *J. Phys. Oceanogr.*, *4*(4), 579–593.

Wilheit, T., & Chang, A. (1980). An algorithm for retrieval of ocean surface and atmospheric parameters from the observations of the scanning multichannel microwave radiometer. *Radio Science*, *15*(3), 525–544.

Wu, J. (1979, sep). Oceanic Whitecaps and Sea State. *J. Phys. Oceanogr.*, *9*(5), 1064–1068.

Yin, X., Boutin, J., Dinnat, E., Song, Q., & Martin, A. (2016). Roughness and foam signature on smos-miras brightness temperatures: A semi-theoretical approach. *Remote sensing of environment*, *180*, 221–233.

Yin, X., Boutin, J., Martin, N., & Spurgeon, P. (2012, may). Optimization of L-Band Sea Surface Emissivity Models Deduced From SMOS Data. *IEEE Transactions on Geoscience and Remote Sensing*, *50*(5), 1414–1426.

Yueh, S. (1997). Modeling of wind direction signals in polarimetric sea surface brightness temperatures. *IEEE Transactions on Geoscience and Remote Sensing*, *35*(6), 1400–1418.

Zhang, L., Shi, H., Wang, Z., Yu, H., Yin, X., & Liao, Q. (2018). Comparison of wind speeds from spaceborne microwave radiometers with in situ observations and ecmwf data over the global ocean. *Remote Sensing*, *10*(3), 425.

Zhou, Y., Lang, R. H., Dinnat, E. P., & Le Vine, D. M. (2017). L-band model function of the dielectric constant of seawater. *IEEE Transactions on Geoscience and Remote Sensing*, *55*(12), 6964–6974.